J|A|C|S
ARTICLES

Published on Web 02/03/2009

Synthesis and Magnetic and Charge-Transport Properties of the Correlated 4d Post-Perovskite $CaRhO_3$

Kazunari Yamaura,*[,†,⊥] Yuichi Shirako,[‡] Hiroshi Kojitani,[‡] Masao Arai,[§] David P. Young,[||] Masaki Akaogi,[‡] Mamoru Nakashima,[‡] Tetsuhiro Katsumata,[‡] Yoshiyuki Inaguma,[‡] and Eiji Takayama-Muromachi[†,⊥,#]

Superconducting Materials Center, National Institute for Materials Science, 1-1 Namiki, Tsukuba, Ibaraki 305-0044, Japan, JST, Transformative Research-Project on Iron Pnictides (TRIP), Tsukuba, Ibaraki 305-0044, Japan, Department of Chemistry, Gakushuin University, 1-5-1 Mejiro, Toshima-ku, Tokyo 171-8588, Japan, Computational Materials Science Center, National Institute for Materials Science, 1-1 Namiki, Tsukuba, Ibaraki 305-0044, Japan, Department of Physics and Astronomy, Louisiana State University, Baton Rouge, Louisiana 70803, and International Center for Materials Nanoarchitectonics (MANA), National Institute for Materials Science, Tsukuba, Ibaraki 305-0044, Japan

Received November 24, 2008; E-mail: YAMAURA.Kazunari@nims.go.jp

Abstract: A high-quality polycrystalline sample of the correlated 4d post-perovskite $CaRhO_3$ (Rh^{4+}: $4d^5$, $S_{el} = 1/2$) was attained under a moderate pressure of 6 GPa. Since the post-perovskite is quenchable at ambient pressure/temperature, it can be a valuable analogue of the post-perovskite $MgSiO_3$ (stable higher than 120 GPa and unstable at ambient pressure), which is a significant key material in earth science. The sample was subjected for measurements of charge-transport and magnetic properties. The data clearly indicate it goes into an antiferromagnetically ordered state below ~90 K in an unusual way, in striking contrast to what was observed for the perovskite phase. The post-perovskite $CaRhO_3$ offers future opportunities for correlated electrons science as well as earth science.

I. Introduction

Since a post-perovskite transition was discovered in $MgSiO_3$ in a laser-heated diamond anvil cell,[1] vast attention has been focused on the transition. It likely plays a pivotal role in the cause of D" seismic discontinuity in the lowermost few hundred kilometers of the earth's mantle.[2] Experimental determination of pressure/temperature variation in the D" layer is expected to be achieved by further studies of the post-perovskite $MgSiO_3$, which may promote understanding of our planet. The post-perovskite is thus believed highly significant in deep earth science; however, it is stable only under extreme conditions, higher than 120 GPa/2200 °C, restricting progress of the studies. Besides, the post-perovskite $MgSiO_3$ is unquenchable, stunting the studies as well. It is, therefore, intensely desired to establish an analogue oxide that is helpful for the studies.

To the best of our knowledge, only a few oxides crystallize into a post-perovskite: $CaIrO_3$ can be synthesized without applying high pressure.[3] $CaPtO_3$ is obtainable under a high-pressure/temperature condition and is quenchable at ambient condition,[4,5] while $MgGeO_3$ and $MnGeO_3$ are unquenchable.[6,7] It appears that only two, $CaIrO_3$ and $CaPtO_3$, are available as a post-perovskite at ambient condition. We thus attempted to discover an additional post-perovskite oxide for the past few years, and very recently, we found that the ruthenium oxide $CaRuO_3$ transforms into a post-perovskite under a certain pressure/temperature condition (>21 GPa/900 °C).[8] Although the 4d correlated electrons properties are still under investigation, the post-perovskite $CaRuO_3$ apparently captures additional interest because new prospects regarding correlated 4d electrons can be expected. A post-perovskite having correlated d electrons is potentially significant not only in earth science but also in materials science. In fact, a recent study on the 5d post-perovskite $Ca_{1-x}Na_xIrO_3$ revealed the appearance of a metal−insulator transition.[9]

Moreover, we found that the perovskite $CaRhO_3$[10] transforms into a post-perovskite as does the perovskite $CaRuO_3$ in a 6−8 Kawai-type multianvil apparatus.[11] The post-perovskite $CaRhO_3$

† Superconducting Materials Center, National Institute for Materials Science.
⊥ JST.
‡ Department of Chemistry, Gakushuin University.
§ Computational Materials Science Center, National Institute for Materials Science.
|| Louisiana State University.
International Center for Materials Nanoarchitectonics (MANA), National Institute for Materials Science.

(1) Murakami, M.; Hirose, K.; Kawamura, K.; Sata, N.; Ohishi, Y. *Science* **2004**, *304*, 855.
(2) Oganov, A. R.; Ono, S. *Nature* **2004**, *430*, 445.
(3) Kojitani, H.; Furukawa, A.; Akaogi, M. *Am. Mineral.* **2007**, *92*, 229.
(4) Ohgushi, K.; Matsushita, Y.; Miyajima, N.; Katsuya, Y.; Tanaka, M.; Izumi, F.; Gotou, H.; Ueda, Y.; Yagi, T. *Phys. Chem. Miner.* **2008**, *35*, 189.
(5) Inaguma, Y.; Hasumi, K.; Yoshida, M.; Ohba, T.; Katsumata, T. *Inorg. Chem.* **2008**, *47*, 1868.
(6) Runge, C. E.; Kubo, A.; Kiefer, B.; Meng, Y.; Prakapenka, V. B.; Shen, G.; Cava, R. J.; Duffy, T. S. *Phys. Chem. Miner.* **2006**, *33*, 699.
(7) Tateno, S.; Hirose, K.; Sata, N.; Ohishi, Y. *Phys. Chem. Miner.* **2006**, *32*, 721.
(8) Kojitani, H.; Shirako, Y.; Akaogi, M. *Phys. Earth Planet. Inter.* **2007**, *165*, 127.

 10.1021/ja8091906 CCC: $40.75 © 2009 American Chemical Society

is quenchable at ambient condition.[11] Subsequently, we determined the pressure−temperature phase diagram of $CaRhO_3$ in a range below 27 GPa.[11] Afterward, we used a belt-type apparatus (maximum pressure was limited up to 6 GPa but has a larger sample room) instead of the Kawai type in order to gain sample mass, which was practically effective to improve the sample quality. Indeed, we succeeded in obtaining a high-quality polycrystalline sample of the newly synthesized post-perovskite $CaRhO_3$ followed by measurements of the magnetic and charge-transport properties. The results clearly demonstrated correlated electrons features, suggesting that the 4d post-perovskite $CaRhO_3$ is worthy of future studies in materials science as well as in geophysical science. To our knowledge, this is the first report on the magnetic properties of the post-perovskite oxide having 4d correlated electrons.

II. Experimental Section

Polycrystalline samples of the post-perovskite and perovskite $CaRhO_3$ were synthesized by a solid-state method from CaO, Rh_2O_3, and $KClO_4$ (99.5%, Kishida Chemical Co.). The Rh_2O_3 powder was prepared by heating Rh powder (3N, Rare Metallic Co.) in oxygen at 900 °C for 24 h. The CaO powder was prepared from $CaCO_3$ (4N, Kanto Chemical Co.) by heating in argon at 1200 °C for 6 h. A mixture of the staring materials at a ratio Ca/Rh/O = 1/1/1.03 was placed into a Pt capsule with a MgO inner, which prevents direct contact between the capsule and the mixture. Preliminary synthesis without the MgO inner resulted in poor sample quality, indicating a significant role of the inner in the synthesis. The capsule was then heated in a belt-type apparatus, which is capable of maintaining 6 GPa during heating. Heating was conducted at 1900 °C for 30 min followed by annealing at a fixed temperature between 800 and 1600 °C for 30 min. The temperature under high pressure was estimated from the magnitude of the electric power supply through a conversion table. After annealing the capsule was quenched in press within a minute before releasing the pressure. Synthesis without annealing was also conducted in the same manner.

Dense and black pellets were obtained at ambient pressure and temperature. Part of the sample was investigated by a powder X-ray diffraction (XRD) method in a commercial apparatus (X'Pert PRO MPD system, PANalytical). Cu Kα radiation was used. Scanning electron microscope/energy-dispersive using X-ray (SEM/EDX) analysis was conducted on a polished surface of a selected sample in a commercial apparatus (JSM-6360, JEOL, equipped with INCA Energy, Oxford Instruments). The acceleration voltage was 15 kV.

Electrical resistivity (ρ) of the pellet was studied by a four-point probe method with a gage current of 0.5 mA. Electrical contacts on the four locations along the rectangular parallelepiped sample were prepared from silver wires and silver paste. Magnetic susceptibility was measured after cooling the sample to 2 K without applying a magnetic field; then the sample was slowly warmed to 400 K (zero-field cooling, ZFC) and again cooled to 2 K in a magnetic field of 10 kOe (field cooling, FC) in a Quantum Design MPMS. Isothermal magnetization was measured in the same apparatus. Specific heat (C_p) measurements were performed in a Quantum Design PPMS by a time-relaxation method with and without applying a magnetic field of 70 kOe. The KCl contribution to each C_p data was subtracted using sets of tabulated data.[12] Thermopower (S) was measured in PPMS. The absolute thermopower of the sample was calculated using the thermopower of constantan measured simultaneously.

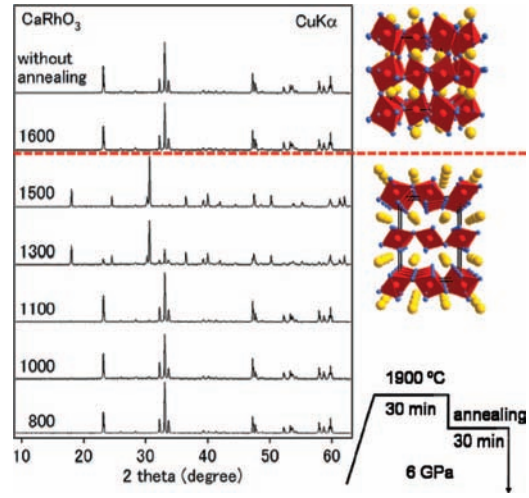

Figure 1. Powder XRD profiles of the $CaRhO_3$ samples annealed at a fixed temperature (indicated on each pattern). The heating diagram is shown at the bottom. Right-side figures are schematic structure view of the perovskite (above the line) and post-perovskite (below the line) based on the results in ref 11. All patterns were taken at ambient pressure and temperature.

III. Results and Discussion

The perovskite $CaRhO_3$ was synthesized at 6 GPa as reported elsewhere,[10] and we found that the perovskite transforms into a post-perovskite by subsequent annealing. Figure 1 shows powder XRD patterns of all samples annealed at various temperatures, showing evolution of the phase change. The number shown on each pattern indicates the annealing temperature at 6 GPa, estimated from actual electric power. The top two patterns are almost identical regardless of the 1600 °C annealing, while an abrupt change is seen at 1500 °C, indicating a boundary between 1500 and 1600 °C. It should be noted that the boundary temperature is slightly higher than what was found in the Kawai-type apparatus,[11] likely due to a technical matter. The XRD patterns also indicate that the sample annealed at 1300 °C consists of both the phases, and the 1100 °C sample and others are dominated by the perovskite phase. This is probably because the annealing period (fixed at 30 min for all) was too short to complete the transition (except at 1500 °C). The phase appearing after annealing is the post-perovskite (discussed later). The relation between the two phases is highly reminiscent of what was found in the analogous compound $CaIrO_3$, which has a positive Clapeyron slope.[3,13,14] The present results, therefore, suggest that the post-perovskite $CaRhO_3$ is practically useful as well as the post-perovskite $CaIrO_3$ for the sake of advanced studies of an unquenchable post-perovskite such as $MgSiO_3$.

(9) Ohgushi, K.; Gotou, H.; Yagi, T.; Kiuchi, Y.; Sakai, F.; Ueda, Y. *Phys. Rev. B* **2006**, *74*, 241104(R).
(10) Yamaura, K.; Takayama-Muromachi, E. *Physica C* **2006**, *445−448*, 54.
(11) Shirako, Y.; Kojitani, H.; Akaogi, M.; Yamaura, K.; Takayama-Muromachi, E. *Phys. Chem. Miner.* Accepted for publication.
(12) Touloukian Y. S.; Buyco E. H. Specific heat Nonmetallic Solids. In *Thermophysical properties of matter*; IFI Plenum: New York, Washington, 1970; Vol. 5.
(13) Hirose, K.; Fujita, Y. *Geophys. Res. Lett.* **2005**, *32*, L13313.
(14) Miyajima, N.; Ohgushi, K.; Ichihara, M.; Yagi, T. *Geophys. Res. Lett.* **2006**, *33*, L12302.

The XRD patterns clearly proved that the post-perovskite $CaRhO_3$ is fairly stable even after removing the applied pressure. The patterns also confirmed that both the perovskite and the post-perovskite samples are of high quality and fairly little impurities are incorporated: all major XRD peaks were well characterized by a comparable unit cell of $CaIrO_3$ with *Cmcm* (post-perovskite) and *Pnma* (perovskite) symmetry.[3] The quality of the post-perovskite sample was further examined in a SEM/EDX analysis: only Ca, Rh, and O spectra were confirmed beyond the EDX background. Mean particles size is on the order of a few micrometers. Any trace suggesting additional elements was not detected at all from the particles.

Parts of both samples were carefully ground and rinsed in water in a sonic bath for a few minutes to remove KCl residue followed by repeating the rinse 2 times. The powders were dried in air and subjected to an additional structure study by the Reitveld method using Cr Kα radiation. The program RIETAN-2000 was used in the study; detailed results and discussion are given elsewhere.[11] We note here only the principal results: refined parameters of the unit cell are $a = 3.1013(1)$ Å, $b = 9.8555(2)$ Å, and $c = 7.2643(1)$ Å for the post-perovskite (*Cmcm*) and $a = 5.5631(1)$ Å, $b = 7.6309(1)$ Å, and $c = 5.3267(1)$ Å for the perovskite (*Pnma*). *R* factors were 10.98% (12.08%) for R_{wp}, 6.71% (7.50%) for R_e, and 1.64 (1.61) for the goodness of fit for the post-perovskite (perovskite), indicating high quality. The calculated density of the post-perovskite was found to be 1.8% larger than that of the perovskite, comparable to 1.4% for $CaIrO_3$,[3] 1.7% for $CaRuO_3$,[8] and 1.0−1.2% for $MgSiO_3$.[1] The 1−2% density increment is likely a common feature of the post-perovskite transition in oxides.

Schematic structure views were drawn based on the results in Figure 1. It is obvious that the 3-dimensinal (3D) perovskite structure transforms into a layered structure in which RhO_6 octahedra are connected by shearing the edge along the *a* axis and the corner along the *c* axis. The Rh−O layer stacks up alternatively with the Ca layer along the *b* axis. The characteristic structure suggests electronic anisotropy toward 2D, which may be essential for quantum magnetism including unusual superconductivity.

As it is widely accepted, perovskite oxides are extremely rich regarding correlated electrons properties, such as colossal magneto-resistance, high-T_c superconductivity, and room-temperature ferromagnetism. However, a post-perovskite oxide has not yet been sufficiently explored, although it can be rich as well. To date, a few post-perovskite oxides are electronically active to our knowledge: $CaRuO_3$ (Ru^{4+}: $4d^4$, $S_{el} = 1$)[8] and $CaIrO_3$ (Ir^{4+}: $5d^5$, $S_{el} = 1/2$).[9] We thus decided to investigate the magnetic and charge-transport properties of the newly synthesized post-perovskite $CaRhO_3$ (Rh^{4+}: $4d^5$, $S_{el} = 1/2$) because it should be electronically active.

First, we studied the charge-transport properties of both the perovskite and the post-perovskite phases of $CaRhO_3$. Figure 2 shows the temperature dependence of ρ (main panel) and *S* (inset). The resistivity of the perovskite changes monotonically with a positive slope over the whole temperature range (data taken from ref 10), while the thermopower varies to zero on cooling almost lineally. The independent data are consistent with what is expected for a metal. In contrast, the post-perovskite shows a rather semiconducting behavior in electrical resistivity with a negative slope. The thermopower features are more complicated; it changes sign at ∼220 K on cooling and reaches a minimum at ∼90 K with a relatively large magnitude (>|100| mV/K). The sign switch probably reflects a delicate balance

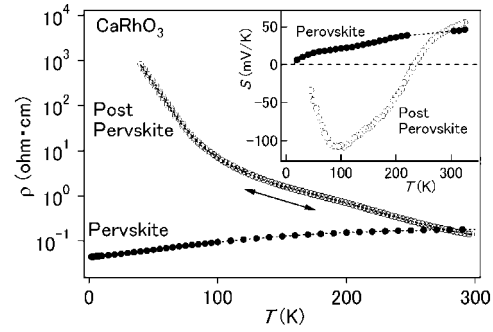

Figure 2. Electrical resistivity and Seebeck coefficient of the polycrystalline samples of the perovskite phase (solid circles) and post-perovskite phase (open circles) of $CaRhO_3$.

between the densities of positively and negatively charged carriers, which is absent in the perovskite phase, indicating that the electronic state is radically changed through the structure transition.

Although contributions from the grain boundary and undetected small impurities are unavoidable in a polycrystalline sample in nature, those are unlikely to account for the nonmetallic behavior in electrical resistivity of the post-perovskite phase because of the thermopower feature. We conclude that the post-perovskite $CaRhO_3$ is nonmetallic in nature. Graphical analysis of the Arrhenius plot (not shown here) of the post-perovskite resistivity data indicated that the activation energy is approximately 38 meV. In addition, the resistivity data follows a variable range hopping scheme rather than a regular hopping scheme, suggesting that randomness plays a significant role in the charge transport. It is highly possible that the reduced electronic dimensionality makes the charge transport more sensitive to such randomness.

The absolute thermopower of the perovskite phase is relatively large among metallic oxides, and the post-perovskite phase also possesses the practical value toward potential applications as well. Unfortunately, we are unable to correctly measure the value in terms of the power factor ($= S^2/\rho$) because of the polycrystalline nature (ρ is higher, leading to underestimation). We can correctly estimate the power factor after single crystals of the compounds are ready for the charge-transport measurements.

Figure 3 shows temperature variation of the magnetic susceptibility of both the phases (top panel) and the isothermal magnetization of the post-perovskite phase (bottom panel). The perovskite shows a paramagnetic behavior down to the limit of 2 K, as reported elsewhere,[10] while the post-perovskite shows a major change at approximately 90 K. A steep increment accompanied by thermohysteresis suggests that a ferromagnetic-like order is established below the temperature in the post-perovskite phase.

It is notable that the magnetic transition undergoes changes of the thermopower and electrical resistivity as the *S* minimum (ca. −100 μV/K) and slope change in ρ vs *T* occur at the magnetic transition temperature, suggesting that the magnetism and charge transport are coupled to some extent. The nature of the coupling is a future subject to be studied.

Since a nearly linear behavior was found in $1/\chi$ vs *T* above ∼200 K for the post-perovskite (see the inset to the top panel of Figure 3), we applied the Curie−Weiss (CW) law to the linear part in order to parametrize the magnetism. Fits were conducted with and without a temperature-independent paramagnetic term, χ_0. For $\chi_0 = 0$, the best fit yielded $\mu_{eff} = 2.99\ \mu_B$/Rh for the effective moment and $\Theta_W = -1071$ K for the Weiss temper-

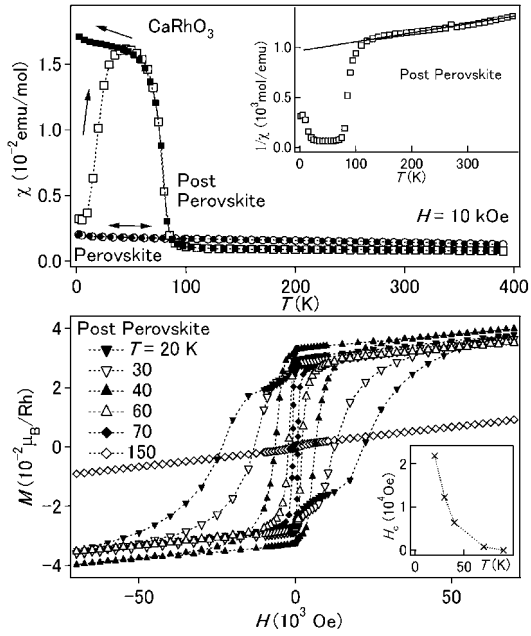

Figure 3. (Top) Temperature dependence of magnetic susceptibility of the post-perovskite phase and perovskite phase of $CaRhO_3$. Open and closed symbols are ZFC and FC data, respectively. (Bottom) Isothermal magnetization curves of the post-perovskite $CaRhO_3$. Insets show alternative plots of the susceptibility data (top) and development of the coercive field (bottom).

ature, suggesting predominantly antiferromagnetic (AF) interactions. It should be noted that the expected spin moment is 1.73 μ_B/Rh ($S_{el} = 1/2$): the large discrepancy between the observed and the calculated spin moments is probably due to a sizable contribution from 4d orbital moments. Alternatively, it is possible that development of short-range magnetic order and magnetic fluctuations on the quasi-2D lattice interfere with the analysis. Further studies using NMR spectroscopy, high-field magnetization, and neutron scatterings are underway. For $\chi_0 \neq 0$, the fit yielded 2.99 μ_B/Rh and -1071 K at $\chi_0 = -1.090 \times 10^{-6}$ emu/mol of Rh, indicating little difference. CW analysis using the linear part only above ~300 K (as a slight slope change is seen) yielded $\mu_{eff} = 2.61$ μ_B/Rh and $\Theta_W = -738$ K regardless of being with and without χ_0.

Isothermal magnetization of the post-perovskite sample was measured at various temperatures, and the magnetization curves are presented in the bottom panel of Figure 3. The data clearly show a small spontaneous magnetization, 0.03 μ_B/Rh, and an accompanied hysteresis. The moment is more than 30 times smaller than the expected moment for an $S = 1/2$ ferromagnetic system. Considering the predominant AF interactions, a weak ferromagnetism (as known as "parasitic ferromagnetism") caused by a noncollinear AF ordering is most likely responsible for the observation. Many possibilities, however, remain as the origin of the magnetism, including Dzyaloshinskii−Moriya interaction, magnetic frustration, and magnetic anisotropy. The issue is left for future study.

Meanwhile, a relatively large magnitude of the coercive field was observed (see the inset to the bottom panel; the field was determined via simple graphical analysis of the hysteresis loop), suggesting anisotropic magnetization of the post-perovskite. Since the grain boundary contribution is somewhat included in the hysteresis loop, further studies using a single crystal would be needed to determine the true magnetic anisotropy of the post-perovskite.

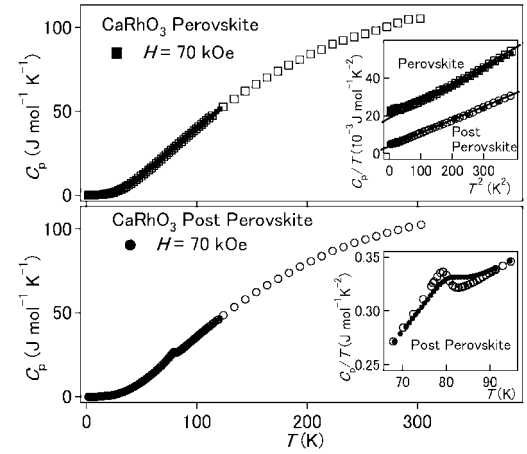

Figure 4. C_p of the perovskite phase (top) and post-perovskite phase (bottom) of $CaRhO_3$. Insets to the top and bottom panels show C_p/T vs T^2 at the low-temperature limit and an expansion of the peak part, respectively.

In order to investigate the magnetic properties further, we measured the C_p of both phases at low temperature. Figure 4 shows the temperature dependence of C_p of the perovskite (top panel) and the post-perovskite (bottom panel) phases. Each measurement was conducted with and without applying a magnetic field of 70 kOe. The data show similar behaviors to a certain extent except a small peak in the vicinity of the magnetic transition temperature. As shown in the inset to the bottom panel, the peak shows field dependence somewhat, clearly indicating that it is magnetic in origin. In order to quantitatively estimate the entropy of the peak part, the main body was subtracted using a polynomial function. After subtraction, an integrated entropy associated with the magnetic transition was estimated to be ~0.25 J mol^{-1} K^{-1}; this corresponds to only 4.4% of R ln 2 (R is the ideal gas constant), expected if whole spins of Rh^{4+} ($4d^5$: $t_{2g}^5 e_g^0$, $S_{el} = 1/2$) are fully ordered. It is likely that much of the entropy is removed via short-range ordering or establishing a low-dimensional magnetism above the magnetic transition temperature. The possibility is also suggested from the CW analysis, as mentioned above.

The inset to the top panel of Figure 4 shows C_p/T vs T^2 at the low-temperature limit. A Sommerfeld coefficient $\gamma = 4.14(6)$ mJ mol^{-1} K^{-2} and a Debye temperature $\Theta_D = 524(1)$ K were inferred for the post-perovskite and $\gamma = 20.5(2)$ mJ mol^{-1} K^{-2} and $\Theta_D = 489(2)$ K for the perovskite from least-squares fits to C_p/T vs T^2 as shown in the inset. The experimental γ is somewhat smaller and larger, respectively, from the calculated γ of ~13 mJ mol^{-1} K^{-2} for both the phases (details of the calculation is in the next paragraph), indicating that the electronic correlation is moderately enhanced in the perovskite and charge transport is somewhat weakened in the post-perovskite. The relatively small magnitude of γ for the post-perovskite is qualitatively consistent with what was observed for the resistivity and thermopower measurements, suggesting that the charge carrier density is lower than the expected density. γ is actually reduced; however, it is noticeable that γ is not absolutely zero, suggesting an alternative possibility that a small amount of charge carriers is practically introduced through oxygen nonstoichiometry. Additional studies including measurements of the Hall coefficient and thermogravimetric analysis would be needed to evaluate the possibilities.

We studied the electronic structure of both phases of $CaRhO_3$ using the local spin density approximation[15] of density func-

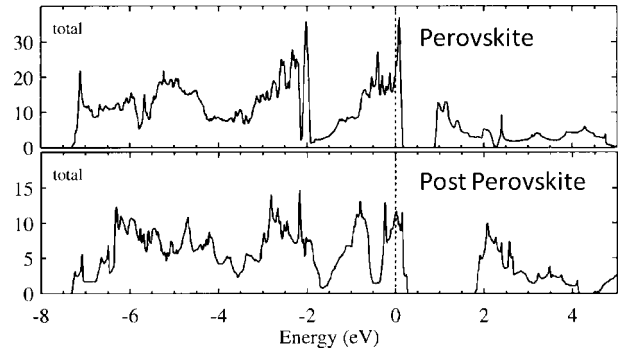

Figure 5. Nonmagnetic DOS of the perovskite phase (top) and post-perovskite phase (bottom) of $CaRhO_3$.

tional theory.[16] We used the WIEN2k package, which is based on a full-potential augmented-plane-wave method.[17] Experimental lattice parameters and atomic coordinates were used for the calculations. The atomic radii were chosen as 2.2, 1.8, and 1.7 au for Ca, Rh, and O, respectively. The cutoff wavenumber K for wave functions in the interstitial region was set to $RK = 7$, where R is the smallest atomic sphere radius. Integration over the Brillouin zone was performed by a tetrahedron method with 60 k points in the irreducible Brillouin zone for the post-perovskite and 36 for the perovskite. The nonmagnetic density of states (DOS) is plotted in Figure 5. Note that the Fermi level is in the DOS structure dominated by the Rh t_{2g} bands (-2 to 0.5 eV), suggesting that the t_{2g} orbitals determine the low-energy properties of $CaRhO_3$ whether the perovskite or post-perovskite. In more detail, the calculated Fermi energy of the post-perovskite lies near the major peak in the DOS structure, suggesting magnetic instability. However, a reasonable magnetic DOS solution is not attained yet: further efforts are directed to the issue.

IV. Conclusions

A high-quality polycrystalline sample of the correlated 4d post-perovskite $CaRhO_3$ was attained under a relatively moderate pressure of 6 GPa, and magnetic and charge-transport properties of the post-perovskite phase were revealed for the first time. The rather practical synthesis conditions and high quality of the sample suggest that the post-perovskite $CaRhO_3$ possesses values as an analogue of the unquenchable post-perovskite $MgSiO_3$ (stable >120 GPa) regarding study of the D" layer in the lower mantle. The newly synthesized post-perovskite offers future opportunities for experimental studies in earth science. The post-perovskite $CaRhO_3$ also offers intriguing possibilities for materials science since it shows multiple correlated electrons features based on a 2D lattice, which might be essential and indispensable for high-T_c superconductivity.

The first-principals calculation for the electronic structure implied a metallic ground state for the post-perovskite $CaRhO_3$. However, an electrically insulating state was actually observed. In addition, it is largely in contrast to what was found for the perovskite phase. Besides, a magnetically ordered state was found below ~90 K, suggesting that the post-perovskite phase is in a Mott insulator regime as well as the post-perovskite $CaIrO_3$.[9] To the best of our knowledge, very few Rh oxides are in the Mott insulating regime. Reduced γ of the post-perovskite supports the possibility. Since great interest can be expected for a Mott insulator by means of chemical doping and physical compression,[18] we have been attempting those on the post-perovskite $CaRhO_3$.

Acknowledgment. We acknowledge Dr. Tachibana, NIMS, for helpful discussions. This research was supported in part by the World Premier International Research Center (WPI) Initiative on Materials Nanoarchitectonics from MEXT, Japan, Grants-in-Aid for Scientific Research (18655080,20360012) from JSPS, Japan, the Murata Science Foundation, Kyoto, Japan, and the Futaba Memorial Foundation, Mobara, Japan.

JA8091906

(15) Perdew, J. P.; Wang, Y. *Phys. Rev. B* **1992**, *45*, 13244.
(16) Hohenberg, P.; Kohn, W. *Phys. Rev.* **1964**, *136*, B864.
(17) Blaha, P.; Schwarz, K.; Madsen, G. K. H.; Kvasnicka, D.; Luitz, J. *WIEN2k, An Augmented Plane Wave + Local Orbitals Program for Calculating Crystal Properties*; Karlheinz Schwarz, Techn. Universitat Wien: Austria, 2001.
(18) Imada, M.; Fujimori, A.; Tokura, Y. *Rev. Mod. Phys.* **1998**, *70*, 1039.